3.1 Synthesis of hexagonal ferrite powder

Hexagonal ferrite powders have been synthesized by sol-gel auto combustion process. Raw materials like strontium nitrate [$Sr(NO_3)_2$], aluminium nitrate [$Al(NO_3)_3.9H_2O$], iron nitrate [$Fe(NO_3)_3.9H_2O$] and citric acid [$C_6H_8O_7.H_2O$] have been used in the auto combustion process. All the chemicals are from Merck, India (GR grade with 99.9% purity). In all nitrate salts, quantitative metal ion content in the solution is maintained through chemical analysis. The solutions are prepared and the molarities of the solutions are determined. 1M metal nitrate solution of each nitrate salt is prepared and kept separately. Before synthesis, chemical analyses of the solutions is carried out to see the actual metal ion concentration.

3.1.1 Sol-gel auto combustion process

The sol-gel auto combustion method has been used to prepare pure and substituted strontium hexaferrite (SrM). This method leads to synthesize highly reactive and homogeneous nano-sized particles with consuming low external energy, inexpensive method [Yue *et al*. (1999)]. Auto combustion process is recognized as self-propagating method, discovered by Merzhanov from Russia. Since then, it has been widely used to fasten the synthesis of complex materials like high temperature superconductor and ferrites [Nersesyan *et al*. (1998)].

Auto combustion process encloses highly exothermic redox reaction process among metal nitrates and fuel, i.e., organic fuel to synthesize multi-component oxides. Figure 3.1 demonstrates auto combustion process flow diagram for synthesis process of hexaferrite powder. Hexaferrite powders have been synthesized for 10 gm per batch. Briefly to synthesize 10 gm $SrAl_4Fe_8O_{19}$ ferrite, 0.010 mol of strontium nitrate, 0.042 mol of aluminium nitrate and 0.084 mol of iron nitrate are taken. Metal nitrate solutions are mixed

with appropriate molarities and the total amount of metal mol present is 0.137 mol in the solution. Equal mol amount of citric acid is added drop wise into the solution of metal nitrate. The mixture is placed in a glass beaker and continuously stirred for few hrs (Figure 3.2 (a)). To synthesize different substituted $SrAl_4Fe_8O_{19}$ ferrite, required amount of metal nitrate solutions like $Co(NO_3)_2.6H_2O$, $Sn(NO_3)_4$, $Cr(NO_3)_3.6H_2O$, $La(NO_3)_3.6H_2O$, $Sm(NO_3)_3.6H_2O$ and $Y(NO_3)_3 \cdot 6H_2O$ are added into the solution before citric acid addition. To control the pH, ammonia solution (NH_4OH) is mixed into the solution to maintain it at 7. Then, the solution is heat treated by hot plate at constant 80 ^oC and converted it into a gel (Figure 3.2 (b)). Later, the gel is auto-ignited on further heating at about 200 ^oC, and formed a fluffy loose powder (Figure 3.2 (c)). The fluffy powder is ground to obtain nano hexaferrite powder (Figure 3.2 (d)). The burnt ash is calcined at 1100 ^oC for 2 hrs for superior crystallization and uniform allocation of cations in the hexagonal ferrite.

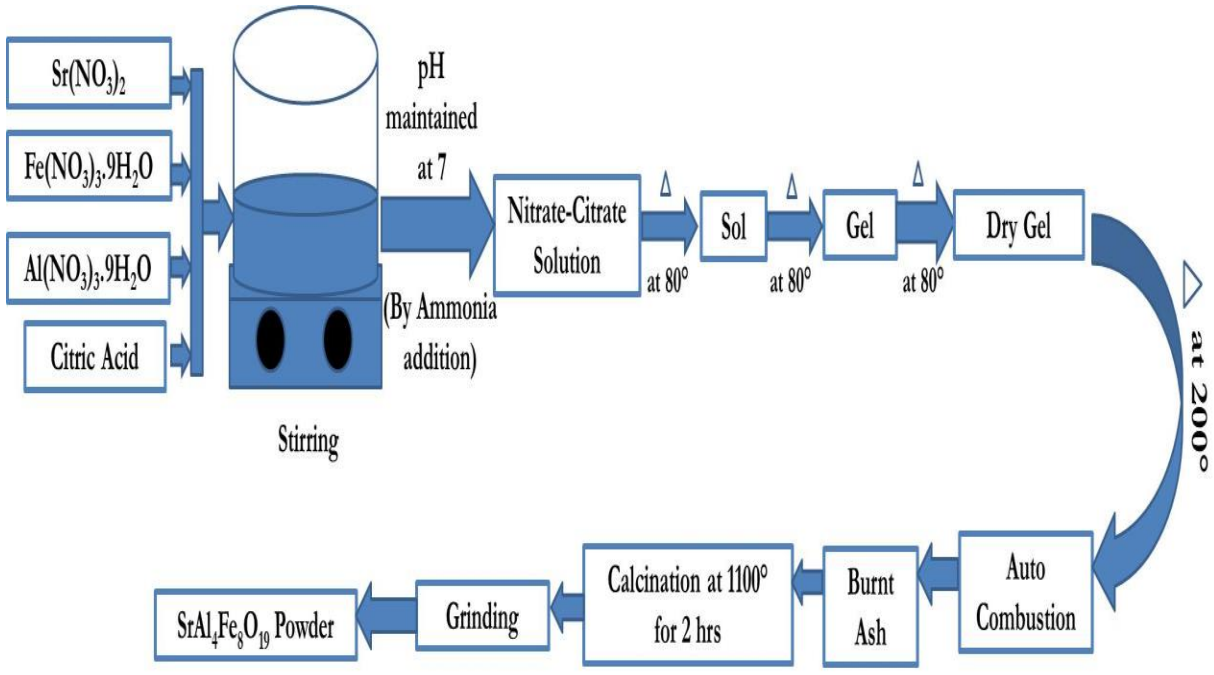

Figure 3.1 Flow diagram of $SrAl_4Fe_8O_{19}$ hexaferrite synthesis process.

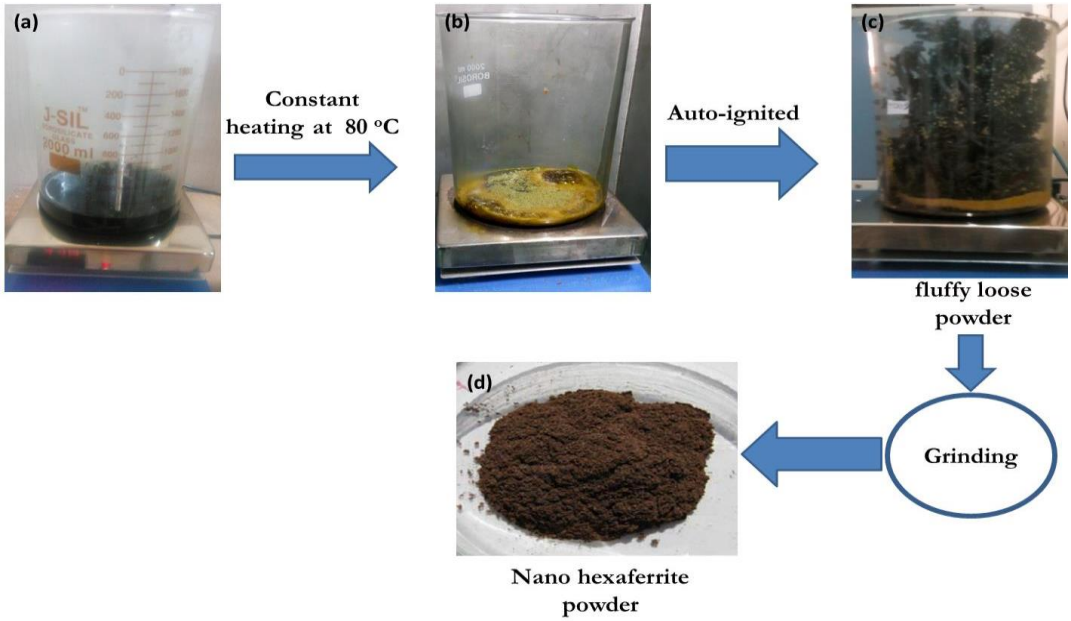

Figure 3.2 Images of (a) metal nitrate-citric acid solution, (b) dried gel, (c) after auto combustion process and (d) As burnt ferrite powder.

3.2 Dried gel and as burnt powder characterization

3.2.1 DTA/TGA analysis

The dried gel of the auto combustion process is characterized by DTA (differential thermal analysis) and TG (thermo gravimetric) analysis using "KEP- Technologies, Setaram-Scientific & Industrial Equipment, France (Model- Labsys, Serial no-560/51920)". In this experiment, dried gel gets heated at 5 °C/min under air atmosphere. α-Al_2O_3 is being used as a reference material and usually take 50 mg of measured sample to investigate. DTA and TG analysis [Jiang (2014)] belongs to a thermo-analytic technique where the prepared material under study along with a reference material which makes to go through identical thermal cycles. The core of a DTA analysis contains holder of reference materials and a sample which are connected through the thermocouple with a furnace and each holder. The measurement is controlled by the heating programs. Temperature differences between the prepared material and reference material are being recorded in a definite atmosphere. In the

duration of thermal progression, phase transition occurs via endothermic or exothermic reaction in the prepared material and identifies with respect to the reference material. If the prepared material goes over a phase transition with increasing in temperature, difference in temperature will illustrate in the thermogram. This plot gives the data about the transformation, i.e., crystallization, melting, glass transitions and phase decompositions. The result has been plotted between the enthalpy and temperature changes. Thermo gravimetric (TG) analysis is the mass loss (or gain) of a sample with a function of temperature. Changes in weight of the sample due to different thermal actions (absorption, desorption, vaporization, sublimation, reduction, oxidation, and decomposition) are considered while the material is exposed to the change in temperature. Therefore, it is applied in the study of gaseous or volatile products lost due to the chemical reactions.

3.2.2 Fourier transform infrared (FTIR) spectroscopy

IR Spectroscopy is used to define the presence of metal–oxygen bond and structure of the synthesize materials [Ganguly *et al*. (2017)]. Each metal–oxygen bond absorbs the characteristic IR radiation frequency. The advantage of FTIR spectroscopy over the other IR Spectroscopy is that this offers a faster and simpler analysis. The FTIR measurements are executed in transmittance mode from 400 to 4000 cm^{-1} at room temperature with BRUKER, TENSOR 27- 3772 FTIR infrared spectrometer, by a resolution with 4 cm^{-1}. Nanoparticles spectra are recorded by forming pellets with 10% KBr powder and direct spectra has been taken for powder samples.

3.2.3 X-ray diffraction analysis

X-ray diffraction is the most used technique to study and identify the atomic structure about the crystalline materials [Stock and Cullity (2001), Jiang (2014)]. X-rays are

described by an electro-magnetic radiation that possess about 10^{-3} to 10 nm wavelength. It is an important tool to study the structure determination. Atoms are set in a well-arranged way and act as a scattering center in the crystal structure of x-rays. It re-emits the x-rays in the identical wavelength as incident radiation at all the directions. The distributed x-rays will be in phase for orderly arranged atoms in a specific direction and it is governed by the atomic spacing and symmetry as shown in Figure 3.3.

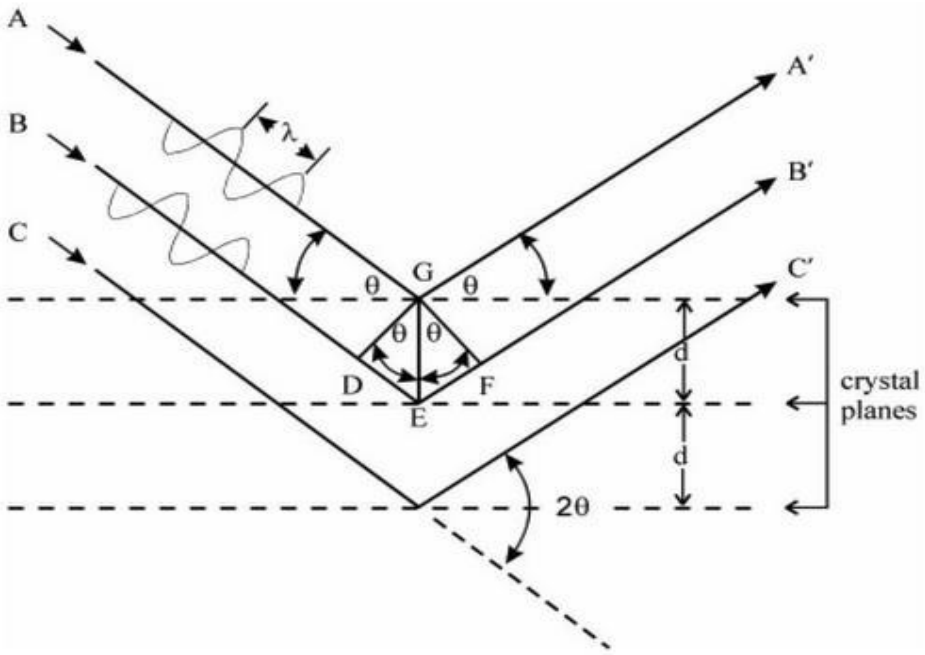

Figure 3.3 A schematic of XRD of regularly spaced atomic planes in a crystal [Jiang (2014)].

On the basis of diffracted beam, symmetry and atomic structure is identified by the following Bragg's law equation:

$$n\lambda = 2\, d\, Sin\, \theta \tag{3.1}$$

Where, λ shows the incident wavelength, θ indicates Bragg's angle with the respect of the crystal planes, d shows atomic spacing and n is the diffraction order. In this present work, the phase formation in the calcined powder is done by using the X-ray diffraction with Cu-Kα

(1.5406 Å) radiation on a RIGAKU- Miniflex II diffractometer (HD20972, Japan). The operating parameters are; 45 kV and 200 mA with the Cu target, with a 0.02 (degree) step size and a count time of 4 s per step. Identifying the formed phases have been done by Philips X-pert high score software which is based on the Hanawalt method. The pattern of the powder is being analyzed by the set of line position (2θ) and their relative intensities (*I)*. Though, angular positions of the lines depend on the incident wavelength and *d*-spacing of lattice planes. Each material is described by their *d* spacing along with their relative intensities, these are sufficient to identify the unknown crystal structure [Cullity (1978)]. The crystallite sizes of burnt ash powder and calcined powder have been calculated by Debye-Scherrer's equation [Cullity (1978)] as follows:

$$t = \frac{0.9\lambda}{\beta Cos\theta} \tag{3.2}$$

Where, t is crystallite size and β is full width at half maxima. Instrument induces the line broadening which has been deducted through the peak width for measuring the crystallite size 't' by using this formula:

$$\beta^2 = \beta_{meas}^2 - \beta_{equip}^2 \tag{3.3}$$

Where, β_{meas} is full width at half maxima of measured peak, β_{equip} is the instrumental broadening, i.e., the standard silicon sample of having β is 0.09821 at 29° (2θ) with (111) hkl. Lattice parameter is calculated by the following relationship for hexagonal system:

$$\frac{1}{d^2} = \frac{4}{3}\left(\frac{h^2+hk+k^2}{a^2}\right) + \frac{l^2}{c^2} \tag{3.4}$$

Where, 'a' and 'c' denotes the lattice parameters and (hkl) are the Miller index.

3.3 Pelletization process of calcined powder

3.3.1 Pellet fabrication process

The calcined ferrite powder is granulated using 3 wt% of polyvinyl alcohol (PVA) solution as a binder and is followed by the following flow chart (Figure 3.4) to fabricate the pellet. After granulation for 2 hrs, the mixed powder is kept for drying at room temperature. Then, the dried powder is sieved through the 300 micron sieve for eliminating the granulation from the powder. The sieved powder is uniaxially pressed with a pressure of 6 tones /cm^2 for 1 minute to form pellets. Pellet dimension is 10 mm diameter (external dia. - D_o) and 2 mm thickness.

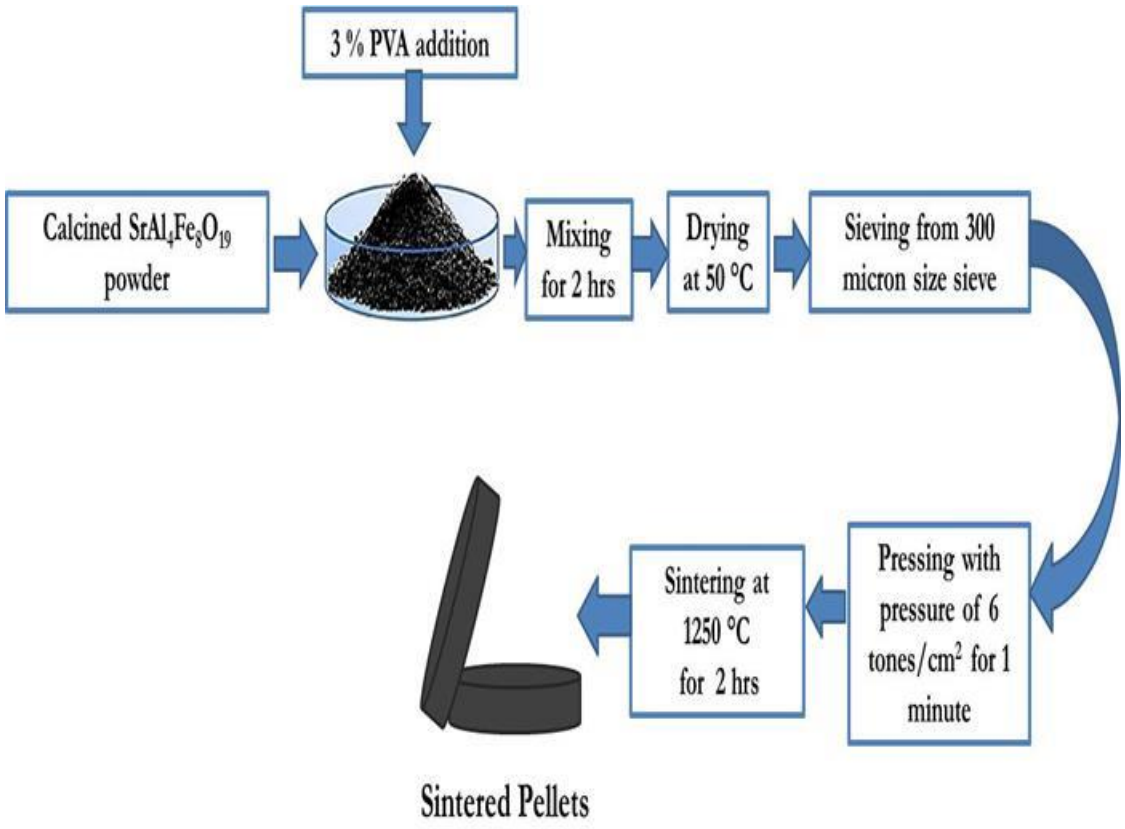

Figure 3.4 Flow chart of the fabrication of hexaferrite pellets.

3.3.2 Sintering process

The pressed sample is being heated into the electric furnace. Figure 3.5 demonstrates the typical sintering cycle. Initially, green pellet is heated with 2 °C/min rate from room temperature to 400 °C followed through soaking for 2 hrs at 400 °C to burn the binder out from the sample. The sample is further heated with 3 °C/min rate up to 1250 °C with soaking for 2 hrs in air atmosphere. After that, cooling is applied on the sample with 3 °C/min rate up to room temperature.

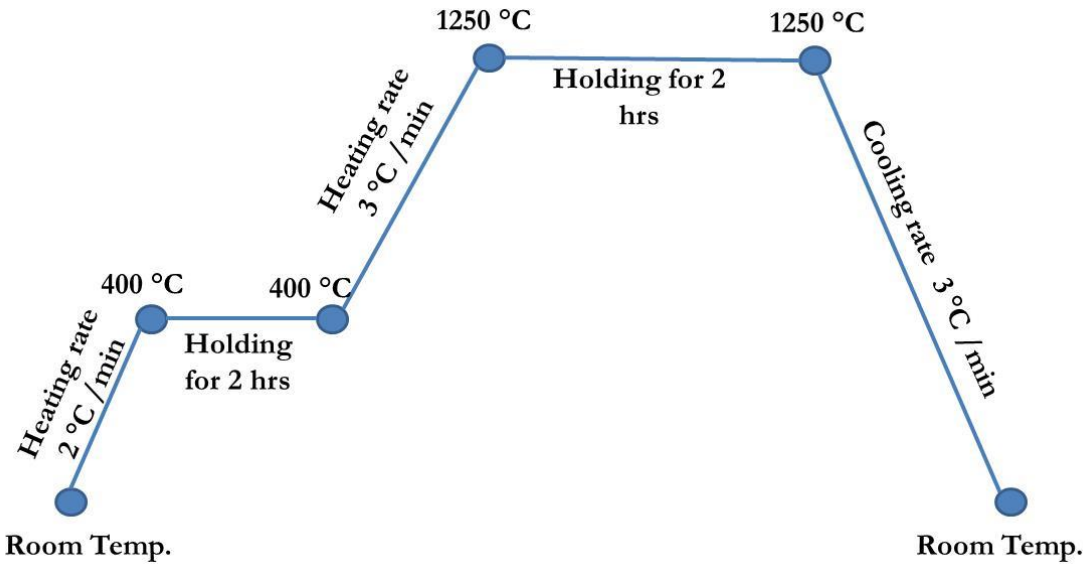

Figure 3.5 A sintering cycle for prepared pellets.

3.4 Characterization of hexaferrite pellets

The physical properties of the sintered hexaferrite pellets have been performed like phase analysis along with structural refinement, microstructural analysis and density measurement. The magnetic, dielectric and resistive properties have been also performed on the sintered hexaferrite pellet.

3.4.1 Density measurement

Bulk densities of the synthesized samples are measured by the well-known Archimede's principle using distilled water as buoyancy liquid. Density of a sample has been measured using a weighing balance having accuracy of 0.0001 g equipped with density measurement kit. The bulk density (D_{Bulk}) is measured by the following formula:

$$D_{Bulk} = \frac{W_D}{W_S - W_A} \tag{3.5}$$

Where, W_D is dry weight, W_S is soaked weight and W_A is suspended weight of the prepared sample.

3.4.2 Scanning electron microscopy (SEM) analysis

Scanning electron microscopy (SEM) is an influential tool to observe the surface morphology such as surface, shape and sizes of the grains and their arrangement [Bozzola and Russell (1998), Hanke (2001)]. SEM delivers greater depth of the field and magnification than the optical microscopes. The SEM microscope is functioning by electronic gun consisting tungsten hot filament which emits electrons. Electrons pass through lenses and become focused. This beam interacts to the sample and excites the electrons of the surface layers. Secondary electrons and backscattered electrons are detected through detector that provides the information about surface morphology of the prepared sample. Scanning Electron Microscopy (SEM), Energy dispersive X-ray Spectroscopy (EDX) and Elemental mapping are performed of the sintered pellets. It has been performed by Scanning Electron Microscope (ZEISS, EVO 18-2045). A thin film of gold (Au) is spluttered onto the pellet surface to elude any charging through SEM analysis. Gold (Au) film thickness is measured by noticing the cross sectional sight of Au film.

3.4.3 Structural refinement analysis

Phase analysis of the sintered sample and their crystallite size determination are recorded by XRD technique. The basics and experimental explanation is explained in section 3.2.3. The rietveld refinement technique has been established by H.M. Rietveld to study the structural info of crystalline materials [Rietveld (1967), (1969)]. Technique of the refinement helps to find out the unknown crystalline structure, number of phases and their percentage in the sample, structural parameter like lattice parameter and their crystallite size. A Rietveld structural refinement has been performed by Fullprof suit program (3.00) software. The software FullProf has been mostly used for performing Rietveld analysis [Rietveld (1969)] of X-ray powder diffraction. The data has been collected at variable or constant step in the angles. Rietveld refinement technique is an automatic programmed and followed the least squares method for refining the theoretical line profile up to it matches with measured profile. Minimized function (ψ) as:

$$\psi = \sum_{i=1}^{n} W_i \, (Y_i^{obs} - Y_i^{calc})^2 \tag{3.6}$$

Where, W_i as assigned weight for i^{th} data points. The refinement justifies on the basis of the obtained difference between calculated profile (Y_i^{cal}) and observed profile (Y_i^{obs}). For good fitting, the difference should be zero. It means that both parameters should overlap to each other, i.e, is Y_i^{obs}-Y_i^{cal} = 0. In refinement, the weight profile residual (R_{wp}), profile residual factor (R_p), chi square (χ^2) and expected profile residual (R_{exp}) is calculated. These factors are as follows:

$$R_P = \frac{\sum_{i=1}^{n} \left| Y_i^{obs} - Y_i^{calc} \right|}{\sum_{i=1}^{n} Y_i^{obs}} \, X \, 100\% \tag{3.7}$$

$$R_{WP} = \left[\frac{\sum_{i=1}^{n} W_i \left(Y_i^{obs} - Y_i^{calc} \right)^2}{\sum_{i=1}^{n} W_i \left(Y_i^{calc} \right)^2} \right]^{1/2} X \, 100\% \tag{3.8}$$

$$R_{exp} = \left[\frac{n-p}{\sum_{i=1}^{n} W_i \left(Y_i^{calc}\right)^2}\right]^2 X\ 100\% \quad (3.9)$$

$$x^2 = \frac{\sum_{i=1}^{n} W_i \left(Y_i^{obs} - Y_i^{calc}\right)^2}{n-p} = \left[\frac{R_{wp}}{R_{exp}}\right]^2 \quad (3.10)$$

For best fitting χ^2 should be close to 1. Rietveld refinement is a process for refinement; thus, an initial estimate of the crystal structure is necessary. Prior information about the structure, its chemistry must be collected from additional methods including first principles techniques, chemical composition analysis and synthesis. This method uses the total pattern fitting along with a least squares method for matching the measured profile and a theoretical line profile. The method performs two models which are the reflections in kind of instrumental functions and the approximate positions of atoms. It is calculated for θ_i position by following equation:

$$Y_i(calc) = \sum_{j=1}^{\text{N phases}} \frac{f_i}{V_j^2} \sum_{k=1}^{N\ peaks} \left|F_{kj}\right|^2 L_K P_{Kj} S_j \left(2\theta_i - 2\theta_{kj}\right) A_j + yb_i(obs) \quad (3.11)$$

Intensity at θ_i is the contribution of phases and all over reflections. From equation (3.11) yb_i, P_{kj}, S_j, A_j, L_k are parameters associated with background, polarization, scale factor, absorption and Lorentz factor, respectively. The parameters V_j and f_j are the volume of the respective phase and atomic form factor. The profile of every reflection is calculated by the $2\theta_i$ - $2\theta_{kj}$, i.e., profile function. In powder diffraction, Caglioti *et al*. (1958) have reported that full width at half maximum (FWHM), i.e., β can be expressed by the tanθ quadratic, if the line profiles breadths vary smoothly, as given by:

$$\beta^2 = U \tan^2\theta + V \tan\theta + W \quad (3.12)$$

Where, U,V as well as W are related to refinable peak shape factors. Many peak shapes function are being used in powder diffraction method like Lorentzian, Gaussian, and Pearson VII or pseudo-Voigt. Function of pseudo-Voigt is a mixture of Lorentzian as well as

Gaussian functions [Wertheim *et al*. (1974), Thompson *et al*. (1987), Young (1993), Cusker *et al*. (1999)]. At lower scattering angle, suggest peak asymmetry due to geometry measurement can be calibrated or refined [Thompson *et al*. (1987)]. Furthermore, peak reflections broadening are associated with the crystallite size as well as micro-strains induce in a material. Crystallite size can be examined by Debye-Scherrer's equation (3.2) [Scherrer and Gesell (1918)]. The micro-strain is exhibited through Stokes and Wilson equation, that is related to peak broadening as given by [Stokes and Wilson (1944)]:

$$\epsilon_{strain} = \frac{\beta}{4 \tan \theta} \tag{3.13}$$

Where, β is the full width at half maxima of a given hkl reflection and ϵ_{strain} is the average strain. Further, Williamson and Hall suggests a method for calculating the strain as well as size broadening by observing the peak width and by way of a peak position function. The analysis deliberates with micro-strain of X-ray line broadening and crystallite size as:

$$\beta_{total} = \beta_{particle\ size} + \beta_{strain} \tag{3.14}$$

Substituting of the integral breadths from Stokes and Wilson's observations and the Scherrer equation, the concluding Williamson-Hall equation is gained when it is multiplied by cosθ on the both sides of the equation [Ungar and Borbely (1996)]:

$$\beta_{total}\ cos\theta = \frac{0.9\lambda}{t} + 4\ sin\theta\ \epsilon_{strain} \tag{3.15}$$

The strain is calculated from the slope and the crystallite size is extracted through the intercept of the curve of βcosθ versus 4sinθ, as shown in Figure 3.6. The bond length between Fe-O and bond angle of Fe-O-Fe measurements have also been performed by Rietveld refinement technique.

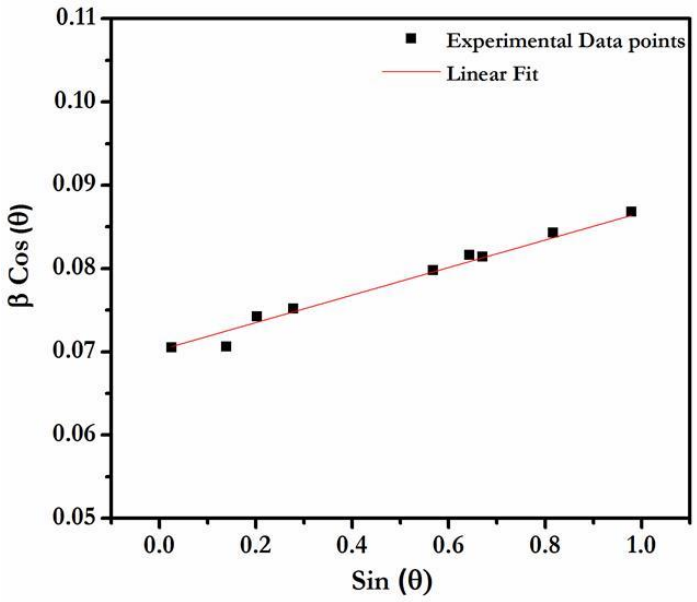

Figure 3.6 Williamson-Hall curve of $\beta\cos\theta$ versus $4\sin\theta$.

3.4.4 Magnetic property measurement system (MPMS) analysis

Magnetic property measurement system (MPMS) is a technique to study the magnetic characterization of the prepared sintered samples. In this work, Quantum design, Model-MPMS 3, EM-QM, USA is used to determine hysteresis curve of all the samples. The maximum magnetic field is applied about 7 Tesla. Magnetic materials get magnetized by applying an external field. Figure 3.7 illustrates the *B*-*H* saturation hysteresis curve. In this figure, it is found that once applied field strength (H)<H_{sat}, it forms a smaller loop [Chikazumi (1969)]. In the Figure 3.7, at the origin state, combined domains totally compensate. With increasing applied field strength, flux density (B) increases along with initial magnetization loop. The B_{sat} (saturation flux density) is achieved at $H = H_{sat}$.

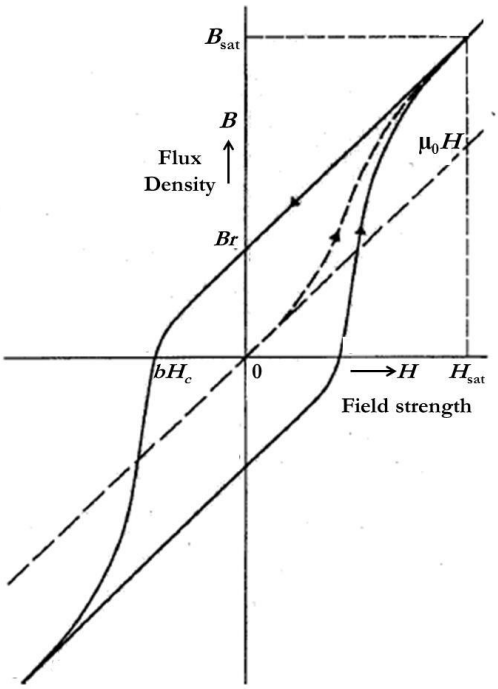

Figure 3.7 Saturation hysteresis curve; flux density (*B*) vs applied field strength (*H*), with $H_{max} > H_{sat.}$ [Hadfield (1962), Chikazumi (1969)].

Saturation state is the state, where, the irreversible mechanisms of magnetization is shattered. Meanwhile, demagnetization and magnetization phenomena are intensely related. H_{sat} is correlated to the iH_c by $H_{sat} \approx 2.5\ iH_c$. The resultant magnetic flux density or induction (*B*) is rest on the applied field strength (*H*) and magnetization (*M*) [Hadfield (1962), Chikazumi (1969)]:

$$B = \mu_0(H + M) = \mu_0 H + J \tag{3.16}$$

Where, *M* and *J* (magnetic polarization) show the involvement of the prepared material. *J* is dependent on *B* as follows:

$$J = B - \mu_0 H \tag{3.17}$$

Figure 3.8 elucidates the hysteresis loop between J vs H along with the original B-H loop. When $H>H_{sat}$, the slope of hysteresis loop comes to zero. When external field become zero then residual magnetic polarization equals to the net remaining flux density, thus $J_r = Br$ [Caig and Clegg (1977)].

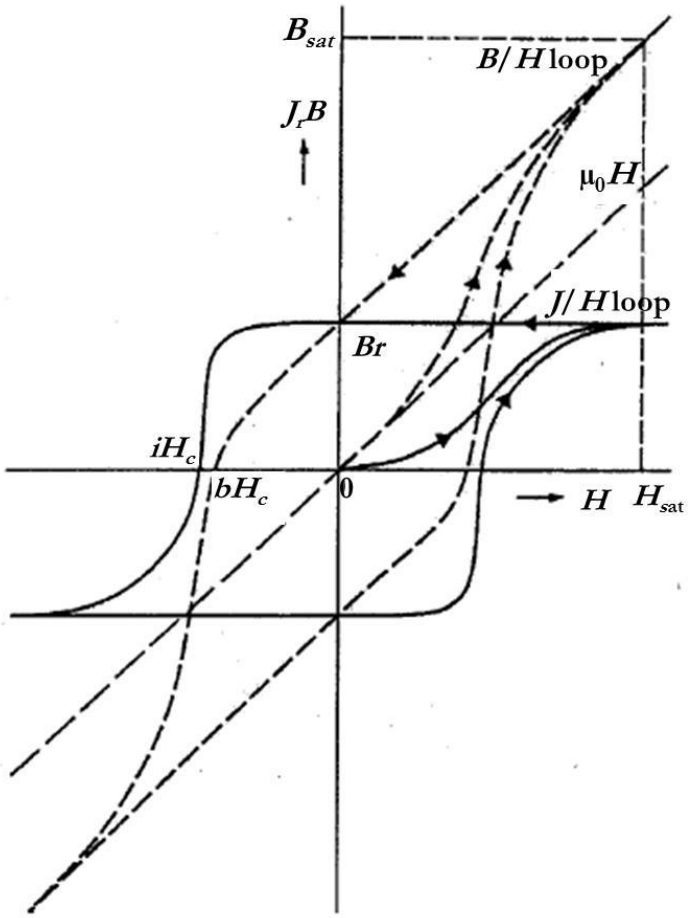

Figure 3.8 Hysteresis loop J vs H as derivative from the B-H loop [Caig M.M. and Clegg (1977)].

The nature of $H>H_{sat}$ is influenced by the degree of alignment. J remain constant once the domain alignment is perfect ($J_{sat} = J$) and J increases through spin rotation, when the domains deviate from the desired direction. After saturation, when the applied field is decreased to zero, B drops to the remanence (Br). The maximum remanence, after magnetization to saturation, is recognized as retentivity. Retentivity and remanence are

regularly used interchangeably; typically with remanence means by retentivity. Since in second quadrant, the applied field increasing in the reverse direction leads to decrease of *B* alongside the demagnetization curve. When *B* becomes zero, the consistent field strength is known as coercive force (bH_c). The coercivity is the maximum coercive force, where, magnetization becomes zero. Commonly, coercive force is meant to coercivity, both terms are frequently used interchangeably. With opposite external field, the polarization (*J*) remains constant up to irreversible demagnetization starts. The opposite field needs to reduce the polarization up to zero is called the polarization coercivity (iH_c). iH_c is always greater than bH_c. The difference between them depends on the squareness ratio as following equation 3.18 [Huang *et al*. (2017)]:

$$\text{squareness ratio} = \frac{H_k}{iH_c} \tag{3.18}$$

Squareness ratio is an important property of the demagnetization plot, being ruled by the "knee" shape. It is the measurement for the squareness, i.e., knee field strength (H_k), which is corresponding to decrease the flux density by 10% with reverence to the remanence [Buschow *et al*. (1993)]. Figure 3.9 shows the typical *B*-*H* demagnetizing curve for permanent magnets. The figure shows second quadrant of *B*-*H* curve and at the right side represents the curve between *BH* vs *B* which indicates the energy product ($(BH)_{max}$) of the magnet [Zijlstra (1982), Buschow *et al*. (1993)]. From the hysteresis curves *Br*, bH_c, iH_c, and $(BH)_{max}$ are measured.

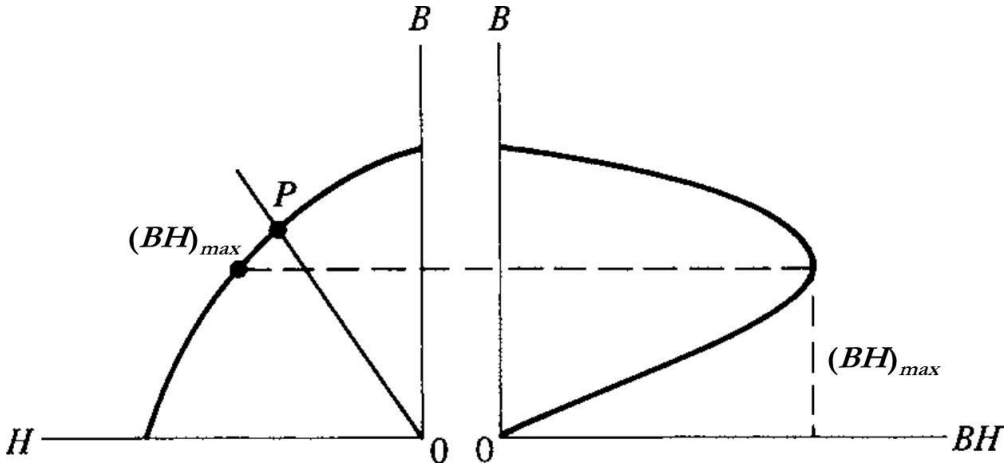

Figure 3.9 Left: demagnetization loop; right: equivalent values of energy product (*B*-*H*) plot on the same *B* scale. $(BH)_{max}$ is shown on both plots [Zijlstra (1982), Buschow *et al*. (1993)].

An important parameter magnetic anisotropy is estimated from the law of approach method to saturation which is founded on the Stroner-Wohlfarth (S-W) model [Verma *et al*. (2016), Almessiere *et al*. (2018)].

$$M(H) = (M_s)\left(1 - \frac{\alpha}{H} - \frac{\phi}{H^2}\right) + \chi_p H \tag{3.19}$$

Where, M_s is saturation magnetization; χ_p is related with high-field susceptibility; α is the anisotropy parameter, which is associated with the structural defect, non-magnetic inclusions and inhomogeneity; ϕ commands the anisotropy. At the region of below Curie temperature or high magnetic field, the term α/H and $\chi_p H$, both can be neglected and ϕ/H^2 gives anisotropy field (H_a) contribution. Thus, this relation can be articulated as below

$$M(H) = (M_s)\left(1 - \frac{\phi}{H^2}\right) \tag{3.20}$$

The linear plot is set between the M *vs* $1/H^2$ plot, as shown in figure 3.10. Where, slope of the linear fitting is ϕ, and intercept is related to M_s. ϕ further express as

$$\gamma = -\frac{1}{15} H_a^2 \tag{3.21}$$

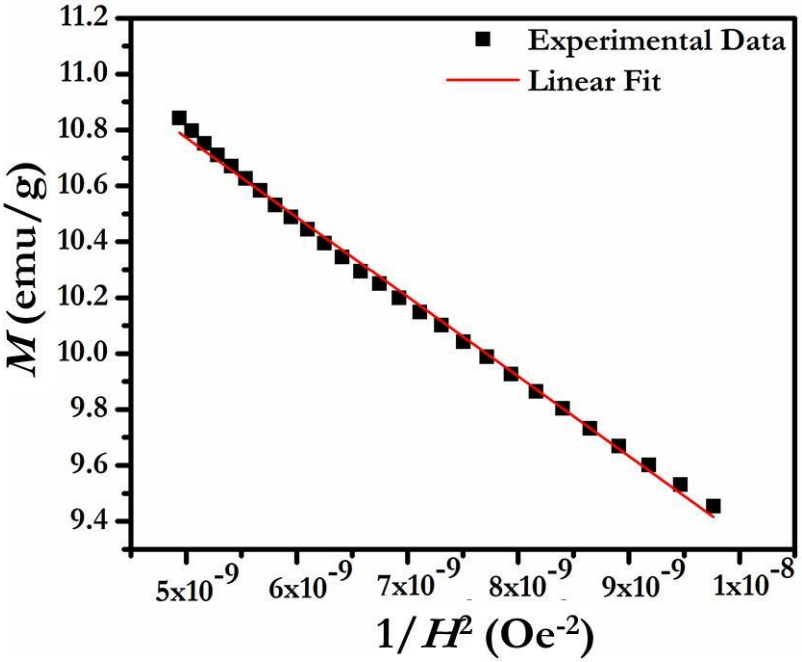

Figure 3.10 The linear plot between M versus $1/H^2$.

Further, H_a can be expressed by:

$$H_a = \frac{2K_{eff}}{M_s} \tag{3.22}$$

Where, K_{eff} is magneto-crystalline anisotropy constant [Verma *et al*. (2016), Mahadevan *et al*. (2017), Almessiere *et al*. (2018)]. Another factor is magnetic moment (Bohr magneton (μ_B)), which is calculated by the following formula [Hilli *et al*. (2012)]

$$\mu_B = \frac{Molecular\ weight\ \text{x}M_s}{5585} \tag{3.23}$$

3.4.5 Impedance measurement

Sintered pellet samples have been used to measure dielectric constant (Ɛ) and resistivity (ρ). Pellet are coated through silver paste to create electrodes as followed by the Figure 3.11. These coated pellets are cured at 300 °C temperature for 30 minutes. Dielectric constant ($\mathcal{E}$) is measured by the following formula [Ashiq *et al*. (2011)]:

$$\varepsilon = \frac{C\,T}{\varepsilon_0\,A} \tag{3.24}$$

Where, *C* is capacitance in Farad, A is the pellet cross-sectional area in meters, T is the pellet thickness in meters and $Ɛ_0$ is dielectric constant of free space. The Ac resistivity (ρ) is calculated by the following formula [Buchanan (1946)]:

$$\rho = \frac{1}{\omega * \varepsilon_0 * \varepsilon * Tan\,\delta} = \frac{A}{2\pi * f * Tan\delta * C * d} \tag{3.25}$$

Where, ω is angular frequency. The impedance analysis has been carried out by the impedance analyzer (Key Sight Technology, Model-E4990A) in 20 Hz-20 MHz frequency range. The difference of dielectric constant and resistivity with frequency has been plotted. Curie temperature measurements are carried out during heating the sample at a rate of 1 °C per min.

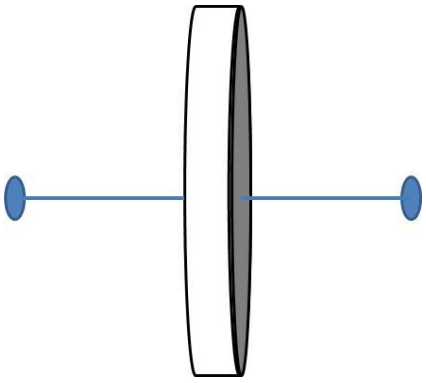

Figure 3.11 Silver coated pellet.